DOMINANT CONDUCTION MECHANISM AND THE EFFECTS OF DEVICE TEMPERATURE ON ELECTRICAL CHARACTERISTICS OF Al/ZnPc/n-Si STRUCTURES

A. Hussain[1*], P. Akhter[2] and A. S. Bhatti[1]

[1]Depaertment of Physics, COMSATS Institute of Information Technology, Islamabad 44000, Pakistan

[2]Pakistan Council of Renewable Energy Technologies, 25, H-9, Islamabad44000, Pakistan

Aluminum/Zinc Phthalocyanine/n-Si metal semiconductor contact with organic interfacial layer have been developed and characterized by Current–Voltage-Temperature (I-V-T) measurements, to study its junction and charge transport properties. The junction parameters, of diode ideality factor (n), barrier height (ϕ_b) and series resistance (R_S), of the device are found to shift with device temperature. The barrier height is found to increase and the series resistance is found to decrease with increasing device temperature, whereas the diode ideality factor increases up to the device temperature of 323K and it decreases for higher device temperatures. The activation energy of the charge carriers is found to be 52meV and the peak of interface state energy distribution curves is found to shift in terms of Ess-Ev value from 0.622 eV to 0.827 eV with increasing device temperature. The data analysis implies that the Fermi level of the organic interfacial layer shifts as function of device temperature. In terms of dominant conduction mechanism, the I-V-T data analysis confirms the fit of data to the relationship log $(IV^4) \propto V^{1/2}$ in the device temperature range of 313K to 343K and the Poole-Frenkel type is found to be the dominant conduction mechanism for the hybrid device.

Keywords: Organic and inorganic semiconductor contact and Schottky barrier height; ideality factor; series resistance, Thermionic emission, Electronic transport in interface structures.

1. Introduction

The features of molecular electronics of being inexpensive, light weight and through away electronics on thin and flexible substrates make it a highly potential area of research for future electronic devices. The stability of organic compounds is another feature of molecular electronics which make them the potential materials to be employed in electronic devices. Electrical properties of molecule/metal and molecule/semiconductor interfaces have been extensively studied in some recent reports [1-5] to understand the charge transfer properties of the organic/inorganic interfaces. The organic semiconductors are often studied as interfacial layers in metal/semiconductor structures, in terms of n, ϕ_B and R_S values, as these semiconductors can structurally be modified to engineer the rectification properties of metal/semiconductor contacts [6-10]. These modified Schottky diodes, based on organic/inorganic interfaces, find their application in number of electronic devices, such as, nuclear detectors [11, 12], organic thin film transistors [13-16] and gas sensors [17].

Dominant conduction mechanism in organic thin films and the organic/inorganic semiconductor interfaces have also been extensively studied and reported in some very recent reports [18-23]. These reports suggest different dominant conduction mechanisms in these organic/inorganic structures, which include space charge limited current [18-20], multi step tunneling recombination current [21], Poole-Frenkel conduction mechanism [22] and Schottky conduction mechanism [23]. Similarly, in case of n, ϕ_B and R_S, the electronic parameters of these organic/inorganic

heterojunctions, different values for similar structures are reported [24]. Therefore, we have developed and studied the Al/ Zinc Phthalocyanine/ N-Silicon/ AuSb (1%) structure to investigate the charge transport properties of these structures. The hybrid structure behaves differently at different device temperatures. The n, ϕ_B and R_S values for the device are determined in the temperature range of 283K to 343K. The determined values were crosschecked by reproducing the respective I-V curves at all device temperatures, by adopting the calculated n, ϕ_B and R_S values in the standard diode equation. Activation energy of charge carries, interface state energy distribution curves as function of device temperature and dominant conduction mechanism in the hybrid structure is also studied reported in this paper.

2. Experimental details

Thin film of ZnPc was deposited by high vacuum sublimation on annealed n-type silicon ⟨100⟩ single crystal wafer (of 6.2×10^{-3} Ω cm resistivity) to fabricate the hybrid heterojunction. The silicon wafer was etched initially by wet chemical etching process to obtain the fresh surface of silicon wafer and to reduce its thickness to 300 microns. The silicon wafer was then cleaned in running de-ionized water, followed by a rinse in HF: H_2O (1:10) solution. Further cleaning of the wafer was carried out with IPA and acetone in an ultrasonic bath. The n-silicon surface was thus prepared and the wafer was loaded into a high vacuum evaporator of Leybold Heraeus A550V, the heat resistive evaporation system. High purity Au-Sb (1% Sb) powder was evaporated on back side of the wafer to obtain an ohmic contact. On the front side of wafer, a layer of ZnPc, of 300nm thickness, was evaporated, with an evaporation rate of 2Å/s. After that, 500nm thick contact of Al on the ZnPc film was deposited through a shadow mask, to obtain the front contact area of 2.83×10^{-1} cm^2. All films were deposited at the base pressure of 2×10^{-6}mbar. The prepared structure of Al/ZnPc/n-Si/Au-Sb(1%) was characterized by I-V-T measurements under dark conditions in the terms of its electrical properties, in the device temperature range of 283K-343K. The device temperature was maintained by using "endocal Refrigerated Circulating Bath" of Neslab Instruments Inc. and the I–V measurements were carried out with KEITHLEY-2420 sourcemeter with GPIB data transfer card.

3. Results and discussions

The Al/ZnPc/n-Si metal semiconductor contact with organic layer was characterized in terms of different interrelated aspects to study its charge transport properties.

3.1 Current–Voltage Characteristics

The semi log plots of the I-V-T data of the device, in device temperature range of 283K to 343K, under forward and reverse bias conditions, are shown in Fig.1. The figure shows rectifying behavior of the device. Assuming that there is a Schottky phenomenon in the device and the net current of the device is due to thermionic emission i.e. the diode is a non-ideal diode. The ideal diode equation [25] for the non-ideal diode can be expressed as [26]:

$$I = I_S \left[\exp \frac{q(V - IR_S)}{nkT} \right] \qquad (1)$$

where n is the diode ideality factor, q is the electronic charge, V is the applied voltage, k is the Boltzmann constant, T is the absolute temperature and I_s is the saturation current given by:

$$I_S = S\,^{*}AT^2 \exp\left(-\frac{q\phi_B}{kT} \right) \qquad (2)$$

where S is the contact area, A^* is the Richardson's constant, equal to 110 A/K^2-cm^2 for n-type Si [25] and ϕ_B is the barrier height.
The n, ϕ_b and R_S values were determined by the standard diode characterization technique i.e. by extrapolating the linear part of semi logarithmic I-V plots to current axis to find the value of reverse saturation current and the value of 'n' and ϕ_b were determined by using Eq. (1) and Eq. (2) respectively. The value of R_S was obtained from the slope of the semi logarithmic I-V plots at all device temperatures. The cross check technique of reproducing the I-V curves, by using the calculated values of n, ϕ_b and R_S in Eq. (1), was used to validate the determined values of n, ϕ_B and R_S parameters at all device temperatures. The good match obtained between the experimental and reproduced I-V curves, at an intermediate device temperature of 313K, is shown in Fig. 2 and the shift in n, ϕ_B and R_S values of the hybrid heterojunction, as a function of device temperature, is shown in Fig. 3, 4 and 5, respectively. As a function of device temperature, the value of "R_S" is found to decrease with increasing device temperature, whereas; the value of ϕ_b is found to increase with increasing device temperature, as shown in Fig. 4 and Fig. 5. This can probably attributed to some shift in the Fermi level of the organic semiconductor, ZnPc in our case, with device temperature. The fact that the barrier height of the device increases from 0.839 eV to 0.939 eV i.e. by 100meV in the device temperature range of 283K to 343K, can probably be attributed to some shift in the Fermi level of the organic semiconductor. Also the fact that the value of diode ideality factor increases up to the device temperature of 323K and then it decreases for higher device temperatures, can probably be attributed to some shift in the proportions of the diffusion and recombination currents.

3.2 Activation energy of the charge carriers

Activation energy of the charge carriers is obtained from the Arrhenius plot of conductivity (σ) as shown in Fig. 6. The conductivity "σ" of the device is affected by the device temperature and this dependence may be represented by the Arrhenius equation as:

$$\sigma = Ae^{\frac{-E_a}{RT}} \qquad (3)$$

where A, the pre-exponential factor, is assumed to be independent of temperature, R is the gas constant and T is the absolute temperature. The equation indicates that the plot of Ln (σ) vs. 1/T should be a straight line with a slope of $-Ea/R$. Therefore, the value of activation energy (E_a) can be calculated by using the slope of the above plot, by the following relation:

$$Slope = -\frac{E_A}{R} \qquad (4)$$

In our case, the activation energy of the charge carriers is found to be 52meV.

3.3 Interface state energy distribution

The interface state energy distribution curves were obtained by using the following relation [27]

$$\frac{1}{n} = \frac{\varepsilon_i}{\varepsilon_i + q^2 N_{SS}\delta} \qquad (5)$$

where n is the ideality factor, Nss is the density of the interface states, εi is the permittivity of interfacial layer, and δ is the thickness of interfacial layer and the energy of interface states is given by:

$$E_{SS} - E_V = q(\phi_e - V) \qquad (6)$$

where Ess is the energy, corresponding to the top of the valence band, at the surface of semiconductor and ϕ_e, is the effective barrier height and is given by:

$$\phi_e = \phi_B + \left(1 - \frac{1}{n}\right)V \qquad (7)$$

We have obtained the Nss values by using the Eq. (5), from the I-V data of device at all device temperatures. The shift in interface state energy distribution curves, as function of device temperature, is shown in Fig. 7.

The peak of interface state energy distribution curves shifts from 0.622 eV to 0.827 eV in terms of Ess-Ev value. Keeping in mind this shift and the shift in the value of barrier height for the heterojunction from 0.782 eV to 0.924 eV, the most probable reason for both of these changes could be the shift in the Fermi level of the organic semiconductor, the ZnPc in our case, with the increasing device temperature from 383K to 343K.

3.4 The dominant conduction mechanism

The I-V-T data analysis in his regard implies that the dominant conduction mechanism is either Schottky type or Poole-Frenkel type, where the logarithm of device current varies linearly with the square root of applied electric field; and the difference of the slopes of these plots, when plotted as a function of 1000/T, passes through the origin[28].

In our case, the relationship log $(IV^4) \propto V^{1/2}$, produces a linear relationship between the current and the square root of applied electric field for the device, as shown in Fig. 8 and the slopes of these plots, when plotted as a function of 1000/T, pass through the origin, as shown in Fig. 9, thus confirming the fit of data to the log $(IV^4) \propto V^{1/2}$ relationship for the device, in the device temperature range of 313K to 343K.

To determine the dominant conduction mechanism, the I-V dependence of the hybrid heterojunction can be written as [28]:

$$I = A\exp(BV^{\frac{1}{2}}) \qquad (8)$$

where

$$B = \frac{440n}{T}\left(\frac{n}{\varepsilon_r d^*}\right)^{\frac{1}{2}} \qquad (9)$$

Here B is in $V^{-1/2}$, d^* is the effective thickness of the film in microns, ε_r is the material dielectric constant and n=1 for Schottky and n=2 for Poole-Frenkel type of conduction mechanism. For Schottky mechanism, A is given by

$$A = SA^*T^2\exp\left(-\frac{\phi_0}{kT}\right) \qquad (10)$$

where “S” is the area of the device, A^* is the Richardson constant and ϕ_0 is the zero-field value of barrier potential energy and for Poole-Frenkel conduction, A is given by

$$A = I_0\exp\left(-\frac{\phi_0}{kT}\right) \qquad (11)$$

where $I_0=G_0V$ in the ordinary PF mechanism. The G_0 is the low-field, high temperature conductance of the sample.

The effective thickness of ZnPc layer, for n=1 in Eq. (9), was determined to be 136nm and 273nm for n=2 in the same equation. The latter result is quite close to expected effective film thickness, as the deposited film thickness was 300nm, as measured through oscillating crystal Film Thickness Monitor (FTM) in the thin film deposition system, thus the Poole-Frenkel type is more likely to be the dominant conduction mechanism of two possible dominant conduction mechanisms.
To further verify these results, the plot of ln (I/T^2) versus $10^3/T$, as shown in Fig. 10, of the I-V-T data of the device was studied. This plot should yield a straight line with a slope of "$-\phi$" (the Schottky barrier potential energy), if Schottky is the dominant conduction mechanism [28]. The "ϕ" values, in our case, come out to be -0.38, whereas, the slope value of ln (I/T^2) versus 1/T plot is determined to be 2.98. Therefore, the values are not comparable and it shows that the Schottky is not the dominant conduction mechanism in the device.

Conclusion

The charge transport properties of Al/Zinc Phthalocyanine /n-Si the metal/molecule interface are found to shift with device temperature. In our case the n, ϕ_B and R_S parameters of the device, as calculated by standard characterization technique, show that the barrier height increases and the series resistance decreases with increasing device temperature, whereas the diode ideality factor increases up to the device temperature of 323K and then it decreases for higher device temperatures. The activation energy of the charge carriers is found to be 52meV. The peak of interface state energy distribution curves shift from 0.622 eV to 0.827 eV in terms of Ess-Ev value and the value of barrier height for the heterojunction shifts from 0.782 eV to 0.924 eV. The data analysis implies that the Fermi level of the organic interfacial layer shifts as function of device temperature. The I-V-T data analysis of the device further implies that the relationship log $(IV^4) \propto V^{1/2}$, produces a linear relationship between the current and the square root of applied electric field and the slopes of these plots, when plotted as a function of 1000/T pass through the origin and hence confirms the fit of data to the log relationship $(IV^4) \propto V^{1/2}$ in the device temperature range of 313K to 343K.

The author acknowledges Higher Education Commission, Pakistan for financial support through "Development of S&T Manpower through Indigenous PhD-300 Scholars" program and Pakistan Council of Renewable Energy Technologies, Islamabad, Pakistan for providing lab facilities.

References

[1] Li Wang, Wei Chen, Andrew Thye Shen Wee, Surface Science Reports, Vol. 63 (2008), p. 465.
[2] B.N. Holland, G. Cabailh, N. Peltekis, C. McGuinness, A.A. Cafolla, I.T. McGovern, Applied Surface Science, Vol. 255 (2008), p. 775.
[3] Sang Wan Cho, Yeonjin Yi, Myungkeun Noh, Mann-Ho Cho, Kyung-Hwa Yoo, Kwangho Jeong, Chung-Nam Whang , Synthetic Metals, Vol. 158 (2008), p. 539.
[4] F. Petraki, V. Papaefthimiou, S. Kennou , Organic Electronics, Vol. 8 (2007), p. 522.
[5] F.S. Tautz , Progress in Surface Science, Vol. 82(2007) 479.
[6] R.L. Van Merhaeghe, W.H. Laflere, F.Cardon, J. Appl. Phys. Vol. 76 (1994), p. 403.
[7] Dietrich R. T. Zahn, Sunggook Park, Thorsten U. Kampen , Vacuum, Vol. 67 (2002), p. 101.
[8] S. Antohe, N. Tomozeiu, S. Gogonea, Phys. Status Solidi (a) Vol. 125 (1991), p. 397.
[9] Haibo Wang, Jun Wang, Haichao Huang, Xuanjun Yan, Donghang Yan, Organic Electronics, Vol. 7 (2006), p. 369.
[10] T. D. Anthopoulos, T. S. Shafai , Journal of Physics and Chemistry of Solids, Vol. 64 (2003), p. 1217.
[11] A. Ray, S.K. Gupta, J.V. Yakhmi , Radiation Measurements, In Press, Accepted Manuscript, Available online 26 October 2008.
[12] Dario Natali, Marco Sampietro, Nuclear Instruments and Methods in Physics Research Section A: Accelerators, Spectrometers, Detectors and Associated Equipment, Vol. 512 (2003), p. 419.
[13] Kihyun Kim, Tae Ho Kwak, Mi Yeon Cho, Jin Woo Lee, Jinsoo Joo , Synthetic Metals, Vol. 158 (2008), p. 553.

[14] Liwei Shang, Ming Liu, Deyu Tu, Lijuan Zhen, Ge Liu, Rui Jia, Liqiang Li, Wenping Hu , Thin Solid Films, Vol. 516 (2008), p. 5093.
[15] Rongbin Ye, Mamoru Baba, Kazunori Suzuki, Kunio Mori , Thin Solid Films, In Press, Accepted Manuscript, Available online 20 November 2008.
[16] X. Liu, Y. Bai, L. Chen, F.X. Wei, X.B. Zhang, X.Y. Jiang, Zh.L. Zhang, Microelectronics Journal, Vol. 38 (2007), p. 919.
[17] Stephen Maldonado, Edgardo García-Berríos, Marc D. Woodka, Bruce S. Brunschwig, Nathan S. Lewis, Sensors and Actuators B: Chemical, Vol. 134 (2008), p. 521.
[18] S. Nespurek, O. Zmeskal, J. Sworakowski, Thin Solid Films, Vol. 516 (2008), p. 8949.
[19] H.S. Soliman, A.A.M. Farag, N.M. Khosifan, M.M. El-Nahass, Thin Solid Films, Vol. 516 (2008), p. 8678.
[20] M.M. El-Nahass, H.M. Zeyada, M.S. Aziz, N.A. El-Ghamaz, Solid-State Electronics, Vol.. 49 (2005), p. 1314.
[21] M.M. El-Nahass, A.M. Farid, A. A.M. Farag, H. A.M. Ali, Vacuum, Vol. 81 (2006), p. 8.
[22] S. Senthilarasu, R. Sathyamoorthy, S.Lalitha, A. subbarayan, Solar Energy Materials and Solar Cells, Vol. 90 (2006), p. 783.
[23] J. Ivanco, T. Haber, R. Resel, F.P. Netzer, M.G. Ramsey, Thin Solid Films, Vol. 514 (2006), p.156.
[24] G. Jorosz, J. Non-Cryst. Solids, Vol..352 (2006), p. 4264.
[25] Sze, S. M., 1936- "Semiconductor devices, physics and technology", JOHN WILEY & SONS, Singapore, 1985, pp. 91, 296, 95.
[26] Mehmet E.nver Aydin, Fahrettin Yakuphanoglu, Jae-Hoon Eom, Do-Hoon Hwang, Physica B, Vol. 387 (2007), p. 239.
[27] A. M. Cowley, S. M.Sze, Appl. Phys. Vol. 36 (1965), p. 3212.
[28] A. E. Rakhshani, Y. Makdisi, X. Methew, J. of Materials Sc.: Materials in Elect. Vol. 8 (1997), p. 207.

Figures

Fig. 1.

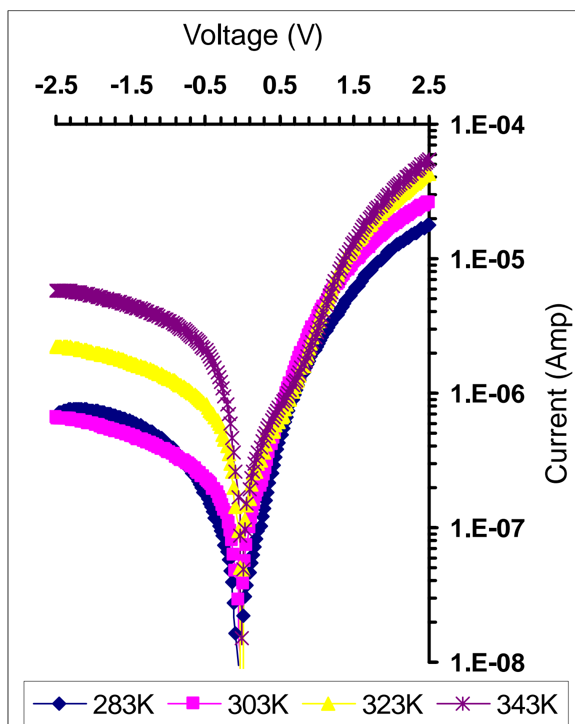

Fig. 2.

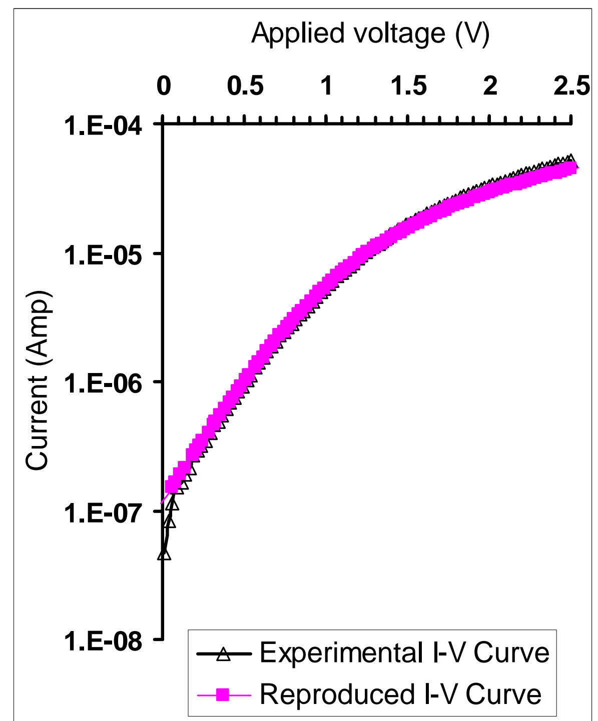

Fig. 3.

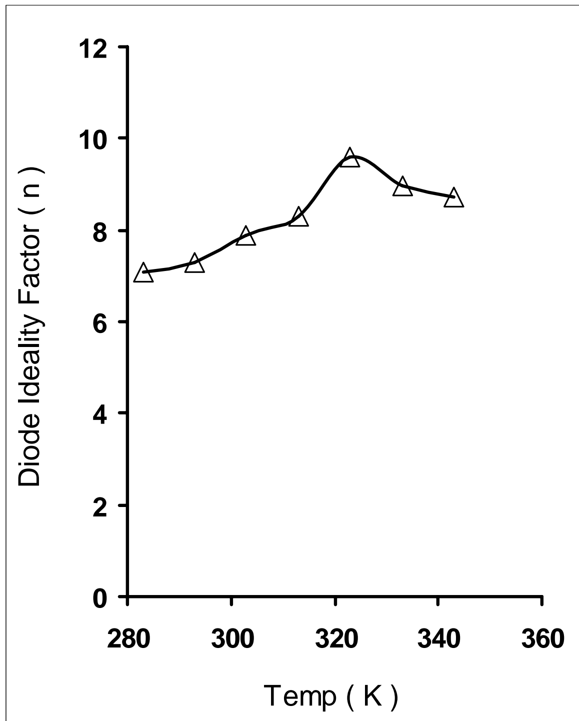

Fig. 4.

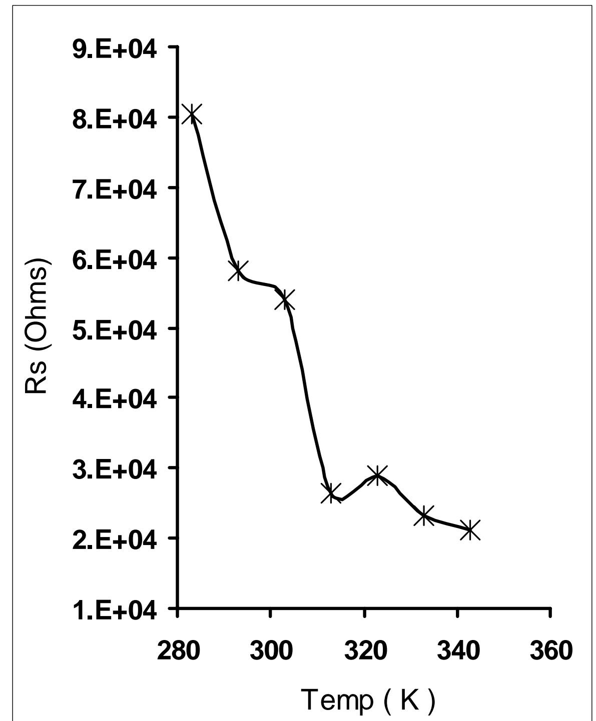

Fig. 6.

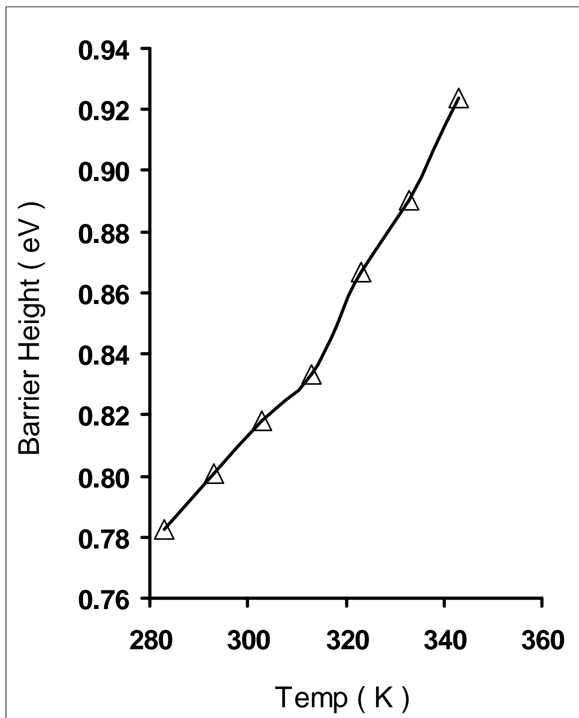

Fig. 5.

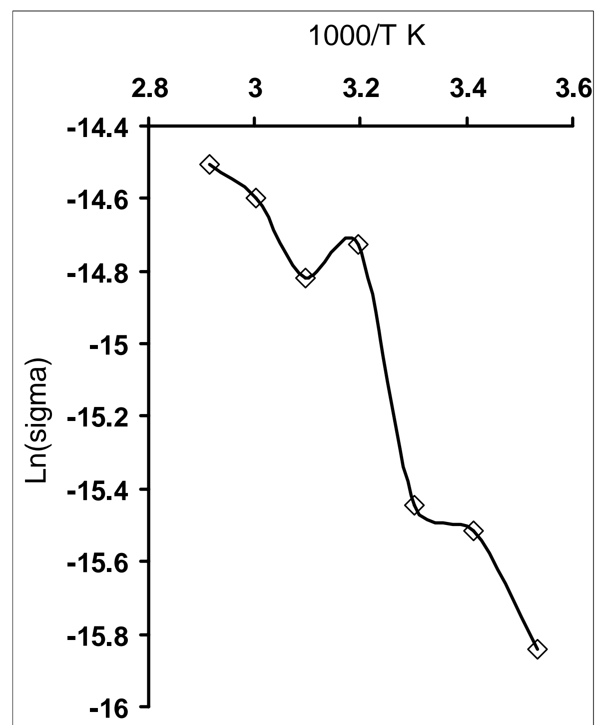

Fig. 7.

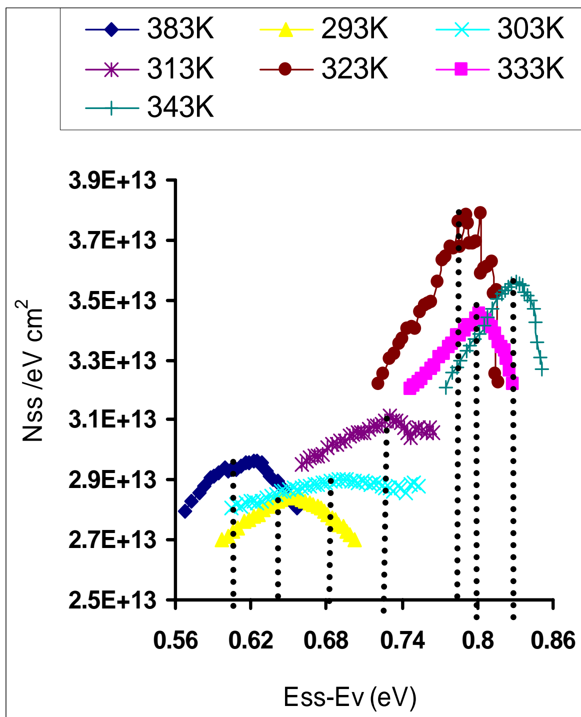

Fig. 8.

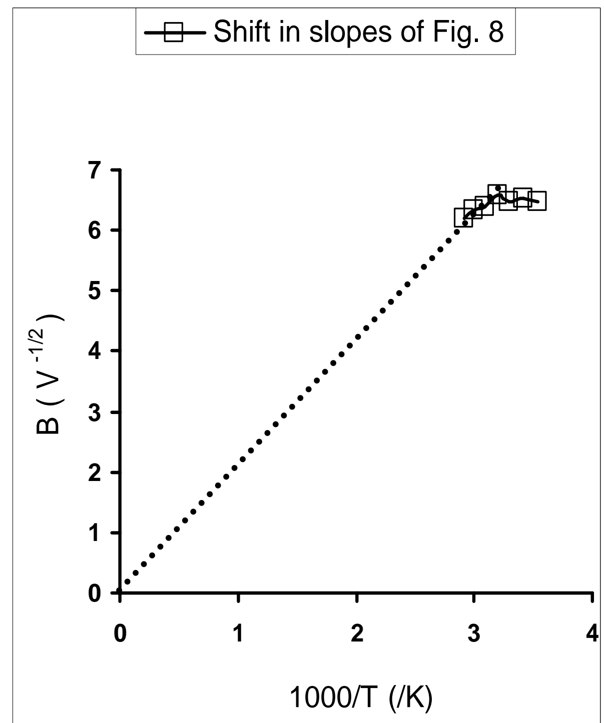

Fig. 10.

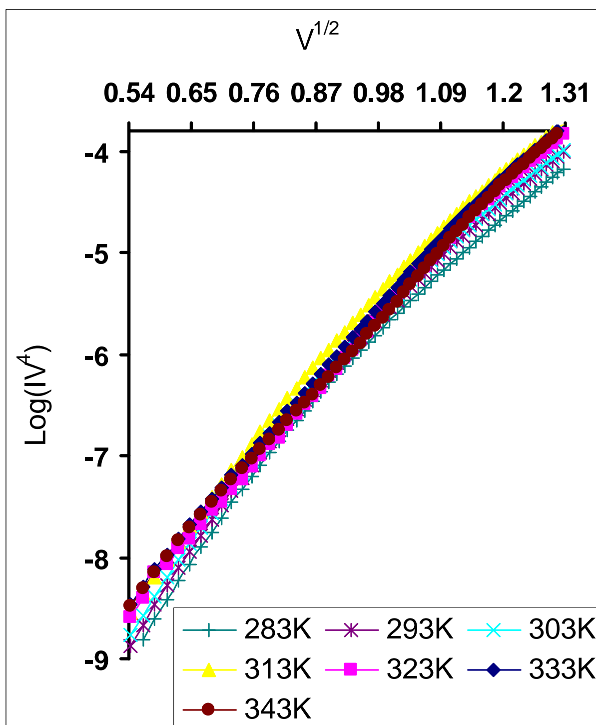

Fig. 9.

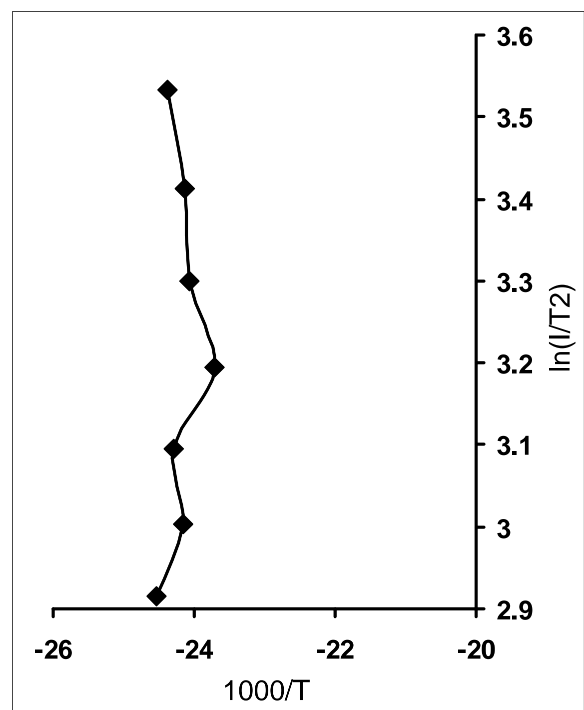

Figure captions

Fig. 1. Semi logarithmic plots of forward and reverse bias I-V characteristics at different temperatures of the Al/ZnPc/n-Si structure.

Fig. 2. Experimental and reproduced (by adopting calculated n, ϕ_b and R_S values in diode equation) forward bias I-V characteristics at 313K of the Al/ZnPc/n-Si structure.

Fig. 3. Plot of diode ideality factor “n” vs. device temperature in the forward bias region of applied voltage of Al/ZnPc/n-Si structure.

Fig. 4. Plot of barrier height ‘ϕ_b’ vs. device temperature in the forward bias region of applied voltage for Al/ZnPc/n-Si structure.

Fig. 5. Plot of series resistance ‘Rs’ vs. device temperature in the forward bias region for applied voltage for Al/ZnPc/n-Si structure.

Fig. 6. Arrhenius plot of conductivity (σ), in the forward bias region of applied voltage, for Al/ZnPc/n-Si structure.

Fig. 7. Plot of N_{SS} vs. E_{SS}-$E_{V,}$ at different device temperatures, for Al/ZnPc/n-Si structure.

Fig. 8. Plot of Log (IV^4) vs. $V^{1/2}$, at different device temperatures, for Al/ZnPc/n-Si structure.

Fig. 9. Plot of measured values of the slope B (as obtained from Fig. 8) vs. $10^3/T$, in the forward bias region of applied voltage, for Al/ZnPc/n-Si structure.

Fig. 10. Plot of ln (I/T^2) vs. 1000/T, in the device temperature range of 283K to 343K, for Al/ZnPc/n-Si structure.